# Scaling and dimensional analysis of acoustic streaming jets.

Valéry Botton, Brahim Moudjed, Daniel Henry, Hamda Ben-Hadid, Jean-Paul Garandet

# *Scaling and dimensional analysis of acoustic streaming jets.*

Valéry Botton[*], Brahim Moudjed[*], Daniel Henry[*], Hamda Ben Hadid[*] and Jean-Paul Garandet[+]

[*] *Laboratoire de Mécanique des Fluides et d'Acoustique, CNRS/Université de Lyon, Ecole Centrale de Lyon/Université Lyon 1/INSA de Lyon, ECL, 36 avenue Guy de Collongue, 69134 Ecully Cedex, France*
[+] *CEA, Laboratoire d'Instrumentation et d'Expérimentation en Mécanique des Fluides et Thermohydraulique, DEN/DANS/DM2S/STMF/LIEFT, CEA-Saclay, F-91191 Gif-sur-Yvette Cedex, France*

## *Keywords*

Acoustic streaming, Eckart streaming, liquid silicon, liquid sodium, acoustic velocimetry

## *Abstract*

The present paper focuses on acoustic streaming free jets. This is to say that progressive acoustic waves are used to generate a steady flow far from any wall. The derivation of governing equations under the form of a non-linear hydrodynamics problem coupled with an acoustic propagation problem is revisited. To do so, a time scale discrimination approach is preferred to the usually invoked amplitude perturbations expansion. This is indeed more consistent with experimental observations of acoustic streaming flows featuring hydrodynamic non-linearities and turbulence. Experimental results are also presented together with a review of former experimental investigations concerning the power-to-velocity relationship for plane ultrasonic transducers in water. A comparison of the shape of the acoustic field with the shape of the velocity field shows that diffraction is a key ingredient in the problem though it is rarely accounted for in the literature. A scaling analysis is made and leads to two scaling laws for the typical velocity level in acoustic streaming free jets; these are both observed in our setup and in former studies by other teams. We also perform a dimensional analysis of this problem: a set of seven dimensionless groups is required to describe a typical acoustic experiment. We find that a full similarity is usually not possible between two acoustic streaming experiments featuring different fluids. We then choose to relax the similarity with respect to sound attenuation and to focus on the case of a scaled water experiment representing an acoustic streaming application in liquid metals, in particular in liquid silicon and in liquid sodium. We show that small acoustic powers can yield relatively high Reynolds numbers and velocity levels; this could be a virtue for heat and mass transfer applications but a drawback for ultrasonic velocimetry.

## *1. Introduction.*

Acoustic streaming flows are steady or quasi-steady flows generated by acoustic waves. Acoustic streaming can be seen as a tool to enhance heat and mass transfer in a number of applications[1–5]. For instance, a number of studies show that ultrasounds used during solidification process can improve final material properties[6–12]. However it can also unwillingly affect some processes. A typical example is that of Acoustic Doppler Velocimetry (ADV) in which ultrasounds are used to measure velocities in a liquid. This technique has been widely used since the late 1990s. It is in particular an efficient way to investigate flows in opaque liquids such as liquid metals[13–23], muddy waters, *etc*. However, a recent investigation shows that, depending on the used settings, commercial ADV systems can

generate significant acoustic streaming flows so that a bias is observed in the measurement itself [24]. This reference study[24] has been performed in water but no guideline is given to assess whether acoustic streaming may significantly affect other configurations, e.g. for the case of liquid metals. Acoustic streaming is present too in both existing and developing medical applications based on high intensity ultrasounds [5,25–27] but also on ultrasounds of lower intensity [28]; the considered liquids are then corporal fluids such as blood or amniotic liquid, the properties of which can significantly differ from that of classical engineering liquids. The discussion developed hereunder might at first order apply to these very peculiar cases but a detailed investigation of them is behind the scope of this paper due to their particular rheology.

Two configurations are often distinguished depending on the scale at which the flow is observed compared to the sound wavelength and the possible interaction of acoustic waves with walls. Schlichting or Rayleigh-Schlichting streaming is due to standing waves, interacting with walls to form acoustic boundary layers of thickness $\delta = (2\nu/\omega)^{1/2}$ where $\nu$ is the kinematic viscosity and $\omega$ is the pulsation of the wave [29]. In this configuration the longitudinal size of observation is on the order of a few wavelengths. An acoustically reflective wall is opposed to the acoustic source so that standing waves occur in the fluid domain. The flow created in the acoustic boundary layers drives a flow in the core of the domain. This flow is observed under the form of recirculations which characteristic scale corresponds to the half-wavelength of the acoustic field. The other configuration is that of Eckart streaming [30]. The present paper is essentially focused on this configuration. Here, the longitudinal size of the observation domain is far greater than the acoustic wavelength; the acoustic waves are progressive and attenuated waves. Eckart streaming is indeed directly due to sound attenuation in the bulk of the fluid through a Reynolds-stresses-like mechanism [31]: The fluid motion can be described as an incompressible flow driven by an external volumetric force which is proportional to the local time-averaged acoustic intensity, $I$, and to the acoustic attenuation coefficient, $\alpha$. An acoustic beam of sufficiently high intensity thus generates a jet flowing in the direction of propagation in the region along the beam axis. In closed cavities, a backflow will also occur for the mass conservation law to be verified.
In the case considered here, the acoustic beam does not interact with the lateral walls, so that no acoustic boundary layer is present in the problem. Nevertheless, even in cases where acoustic boundary layers exist, it can be shown that in large-scale channels (typically with a size of at least one millimeter), the streaming induced by the boundary layers (Rayleigh streaming) is negligible compared with the Eckart streaming[32]. In fact, the "Rayleigh force" is much stronger than the "Eckart force" but it occurs in very thin layers along the boundaries, so that its effect on the streaming is negligible [33,34]. This effect would have some importance only in micro-fluidic devices[32].

Since the pioneering works on the topic, acoustic streaming has very often been presented as a second-order flow. The initially proposed theoretical models leading to the expression of the acoustic streaming force were indeed based on an expansion of each variable in successive approximations. The first order then accounted for the linear acoustic propagation in a quiescent fluid medium, while the second order ruled the acoustic streaming flow[30,33,35]. However, several authors conversely underscored that in many experimental investigations and applications, the observed flow was not of second order[31,36,37]. Experimentalists also observed turbulent acoustic streaming flows, which is not compatible with the assumption of a second order flow, the inertia of which should be negligibly weak[1,31]. The contrast between the efficiency of acoustic streaming in the potential applications cited above and what could be expected from a second order flow is also questionable. Our contention is that a physical

explanation compatible with these experimental observations can be given by considering that the relevant separation of the hydrodynamic problem from the acoustic propagation problem is a time-scales separation rather than an amplitude-scales separation. The frequency of ultrasounds used in liquids is indeed commonly in the Megahertz range or more, which is far greater than the highest frequency component in the considered streaming flows. However, to our knowledge, no derivation of the acoustic streaming force expression has yet been proposed in the existing literature following this path.

A number of experimental papers reports investigations of acoustic streaming flows[4,36,38–40]. The results are all described in dimensional variables and most of these experiments are conducted with water, in which a more or less limited amount of particles is added to serve as tracers. They differ in particular by the size and geometry of the water tank and by the value of the ultrasound frequency and intensity. In some of these papers, experimental results are compared to scaling laws in particular giving the dependence of the fluid velocity on the acoustic power. Most authors expect the observed velocities to scale linearly with the acoustic power, but some of them invoke the proportionality to the power square-root. The assumptions for these expected behaviors to be observed are in addition not explicitly formulated. A common limitation of the literature papers is that they often do not account for diffraction of the acoustic field in their analysis. In particular, a number of them does not pay any attention to the existence of an acoustic near field, which extent can be several times the diameter of the sound source for ultrasonic frequencies in liquids. To the best of our knowledge, dimensional analysis of an acoustic streaming jet has never been reported in any international paper. It is, however, a very efficient tool to reduce the investigated parameters space, but also to design model experiments, convert dimensional observations into more universal non-dimensional form and extrapolate results from one fluid to another. This constitutes in particular the basis of the theory of physical modeling, which allows performing the quantitative conversion of experimental results obtained in a model experiment to a real case featuring potentially another fluid, another size, *etc*. As such, dimensional analysis gives the opportunity to link water experiments reported in the literature and the above mentioned applications. As our team is in particular interested in applications involving liquid metals, another objective of the present paper is thus to investigate the potential of acoustic streaming in some liquid metals.

In the following, the derivation of the acoustic force expression is revisited in section 2 using a time-scale separation approach in which the acoustic streaming flow has not to be assumed of second order. Some basics of linear acoustics are also briefly recalled since the present paper voluntarily takes a hydrodynamics standpoint. The velocity dependence on the acoustic power will be investigated in section 3 using scaling arguments and taking special care to account for acoustic diffraction. Use will be made in section 4 of experimental results from our proper setup[37,41], as well as from former experimental studies of the literature[4,36,38–40], for purposes of comparison and validation. Section 5 will be devoted to the dimensional analysis of the problem and to considerations on the use of the theory of physical modeling in the present framework. The outputs of this section will then be applied to selected liquids in section 6. The considered fluids are chosen in typical applications involving high intensity ultrasounds and ADV: water (to which weakly concentrated suspensions and solutions might be assimilated) and liquid metals, namely liquid silicon and sodium. An important step in this approach is the determination of the sound attenuation coefficient of the considered liquid. This data is actually not always given in usual tables and reference books since its measurement can be difficult in some cases. An additional concern of section 6 is thus to give

guidelines to assess the value of this attenuation coefficient and to properly account for it in a dimensional analysis approach.

## 2. *Physical mechanisms involved in acoustic streaming.*

***An explanation based on time-scales discrimination.***

The approach in the following derivation is to split each variable into an acoustic part, varying rapidly, and a streaming motion part, varying very slowly compared to the acoustic part. The acoustic part will be denoted with a subscript *ac*; it is assumed periodical with zero average over one period $T = 1/f$. The streaming motion part will be denoted with a subscript *s*; due to its slow variations its instantaneous value can be considered equal to its average over one acoustic period, *T*. We start with the continuity and Navier-Stokes equations for a compressible fluid:

$$\frac{\partial \tilde{\rho}}{\partial t} + div(\tilde{\rho}\tilde{\vec{u}}) = 0, \tag{1}$$

$$\tilde{\rho}\frac{d\tilde{\vec{u}}}{dt} = -\overrightarrow{grad}\ \tilde{p} + \mu\nabla^2\tilde{\vec{u}} + \left(\eta + \frac{\mu}{3}\right)\overrightarrow{grad}(div\ \tilde{\vec{u}}), \tag{2}$$

where the tilde (~) denotes any "full" variable before its splitting, $\rho$, $\mu$ and $\eta$ are the fluid density, shear viscosity and bulk viscosity, respectively. The next step is to introduce the split variables in these equations and compute their average over one period of time. The linear terms will then disappear when they feature an acoustic variable (*i.e.* with the subscript *ac*) or be substituted with their instantaneous value when they feature a streaming flow variable (namely those with the subscript *s*). The non-linear terms will disappear when they feature a cross product of an acoustic variable with a streaming flow variable, so that will stay only cross products in which both variables have the same subscript. One can reasonably neglect any variations in viscosity under the effect of the acoustic wave, so that the right-hand side of the Navier-Stokes equation is linear. The left-hand side has terms similar to turbulence Reynolds stresses and thus needs to be developed. After computation, the averaged continuity and Navier-Stokes equations are:

$$\frac{\partial \rho_s}{\partial t} + div(\overline{\rho_{ac}\vec{u}_{ac}}) + div(\rho_s\vec{u}_s) = 0, \tag{3}$$

$$\rho_s\frac{d\vec{u}_s}{dt} = -\overrightarrow{grad}\ p_s + \mu\nabla^2\vec{u}_s + \left(\eta + \frac{\mu}{3}\right)\overrightarrow{grad}(div\ \vec{u}_s) + \overrightarrow{f_{ac}}, \tag{4}$$

where the last term is the acoustic streaming force term has for $i^{th}$ component

$$f_{ac,i} = -\,div(\overline{\rho_{ac} u_{s,i} \vec{u}_{ac}} + \overline{\rho_{ac} u_{ac,i} \vec{u}_s} + \overline{\rho_{ac} u_{ac,i} \vec{u}_{ac}} + \rho_s \overline{u_{ac,i} \vec{u}_{ac}}),\ \text{with } i = 1,\ 2 \text{ or } 3, \tag{5}$$

in a Cartesian work-frame.

A simplifying assumption is that terms proportional to $\rho_{ac}$ in equations (4) and (6) can safely be neglected with respect to terms proportional to $\rho_s$, in particular in liquids. For example, in the case of water, the isentropic compressibility coefficient is $\chi = 5\ 10^{-10}$ Pa$^{-1}$; assuming an acoustic pressure amplitude of $p_{ac} = 3\ 10^5$ Pa, which can be reached in acoustic streaming experiments, the density ratio can be estimated as $\rho_{ac} / \rho_s = 0.015\%$. An additional simplification is made by considering that the obtained streaming flow velocities are always far smaller than the velocity of sound ($c = 1480$ m/s in water), so that the fluid flows at very low Mach number and can be considered as incompressible; in other words, the time and space variations of $\rho_s$ are negligible. Eventually, the obtained set of equations for the acoustic streaming flow is:

$$f_{ac,i} = -\rho_s div(\overline{u_{ac,i} \vec{u}_{ac}}), \tag{6}$$

$$div\, \vec{u}_s = 0, \tag{7}$$

$$\rho_s \frac{d\vec{u}_s}{dt} = -\overrightarrow{grad}\ p_s + \mu \nabla^2 \vec{u}_s + \overrightarrow{f_{ac}}. \tag{8}$$

Let us underscore that the time derivative is not here a partial derivative but a particulate derivative, so that the contribution of streaming flow velocity gradients to inertia terms is effectively present in the left hand side of this formulation. This is an important feature of the present approach as opposed to the derivations based on small perturbations expansions formerly proposed in the literature.

Let us now consider the case of a plane sinusoidal progressive wave propagating with attenuation along the ***x***-direction; with an acoustic velocity amplitude of the form:

$$U_{ac} = \hat{u}_{ac} e^{-\alpha x}. \tag{9}$$

From equation (6), the acoustic streaming force can then be written as:

$$\vec{f}_{ac} = \alpha \rho_s \hat{u}_{ac}^2 e^{-2\alpha x} \vec{x}. \tag{10}$$

As for such a plane wave, the acoustic intensity can be given as[42]:

$$I = \overline{\rho_s c u_{ac}^2} = \frac{1}{2} \rho_s c \hat{u}_{ac}^2 e^{-2\alpha x}, \tag{11}$$

we thus get the following final expression for the force:

$$\vec{f}_{ac} = \frac{2\alpha I}{c} \vec{x}. \tag{12}$$

Such an expression has been previously obtained, but on the basis of a small amplitude expansion approach which to our mind has less physical meaning than the present one. We have indeed shown that the acoustic streaming flow is ruled by the full Navier-Stokes equations for an incompressible fluid. The additional force term, given by equation (12), is the same as that introduced by former authors[31,33,35], but here, the hydrodynamic non-linearity has

not to be introduced *a posteriori* nor artificially in the formulation, as underscored above. The flow is thus the solution to a weakly coupled problem between a hydrodynamic sub-problem and an acoustic propagation sub-problem with both velocities possibly of the same order of magnitude in the two sub-problems. The coupling is made through the force term equation (12), which is proportional to the sound amplitude attenuation coefficient. One interest of this approach is also that the fluid has not been assumed to be at rest in this formulation so that flows driven by other external forces can be accounted for.

The plane wave assumption leading to equation (12) based on eq. (9) corresponds of course to an idealized situation. In practice, it is reasonable to consider such an assumption to be valid in cases where the acoustic wave propagates in a delimited portion of space, namely under the form of a beam. In such cases, the plane wave assumption, equation (9), is considered to hold locally but slow spatial variations of the acoustic velocity amplitude $u_{ac}$ have to be considered, in particular in the transverse direction. The expression "slow spatial variations" can be understood here as variations with a far greater typical length-scale than the acoustic wavelength. As a consequence the expression of the force must be used in conjunction with a propagation model describing the spatial repartition of the acoustic intensity.

The crudest propagation model is to consider an uniform beam of cylindrical shape, which is to say without any diffraction, non-linearity nor attenuation[3,30,43–47]; in this case, attenuation is neglected in the propagation problem and is only accounted for through the attenuation coefficient appearing in the acoustic force expression, equation (12). This leads in particular to 1D analytical solutions to the equations of motions[30,43]. More complex propagation models may account for non-linear effects, diffraction and attenuation[36], which generally necessitate numerical methods. Former investigations[36,37] have shown that diffraction is a key ingredient to reproduce the theoretically observed acoustic streaming velocity profiles, and it will be made clear in the following that our opinion is that diffraction should indeed be accounted for; on the other hand, we have shown that a linear propagation model was sufficient to obtain good results in a range of parameters corresponding at least to our experimental investigation[37,41] which greatly simplifies the handling of the propagation problem. Let us recall that the account of diffraction leads to distinguish a near field and a far field in the acoustic beam emitted by a localized source[42]. The near field is rather complex to handle since it is strongly varying in space and time which requires fine spatial discretization in numerical approaches. The far field on the contrary is the frame of smooth spatial variations and plane waves are considered as a good approximation in this part of the acoustic field. The choice made in the present paper is to restrict the propagation model to linear propagation but to include diffraction as a key ingredient of the problem.

Prior to the scaling and dimensional analysis of this problem, we think useful to recall in the following some basics of linear acoustics in particular concerning attenuation and diffraction. It is an appropriate way to introduce the relevant physical parameters of the propagation sub-problem.

### *Basics of acoustics concerning diffraction*

In the following, the wave is assumed monochromatic so that the acoustic field is fully described by the spatial repartition of the amplitude and the phase of the wave. As expected from the linear theory of a piston source in a semi-infinite medium, its structure exhibits a near field and a far field[42]. Very strong spatial variations occur in the near field, while

smoother variations are seen in the far field. The near filed zone stretches from the acoustic source to the Fresnel length, $L_f$, with :

$$L_f = \frac{D_s^2}{4\lambda}, \tag{13}$$

where $D_s$ is the diameter of the source, and $\lambda = c/f$ is the acoustic wavelength. Note that, at ultrasound frequencies, this near field region can be much longer than the diameter of the source: a source of 3 *cm* in diameter emitting 2MHz ultrasounds in water has, for example, a near field length of $L_f$ =30.4 cm, ten times the source diameter.

In the far field zone, the acoustic beam diameter is larger than the acoustic source diameter because of diffraction. Indeed, the diameter of the sound beam increases linearly so that the sonicated region can be seen as a cone of half-angle $\theta$ such that

$$\sin\theta = 1.22\frac{\lambda}{D_s}. \tag{14}$$

Let us recall from equations (13) and (14) that small diffraction angle means long near field region, since the Fresnel length to diameter ratio, $L_f/D_s$, is inversely proportional to the half angle. Ultrasounds wavelengths in water are commonly less than one millimeter while the sources diameter is of tenth of millimeters. The near field zone is thus often far longer than the source diameter and the diffraction angle is small. As a consequence of the linear increase of the beam diameter, the acoustic intensity rapidly decreases along the longitudinal axis of the beam. Neglecting attenuation, this decrease behaves as $1/x^2$ in the asymptotically far field.

***Basics of acoustics concerning attenuation in liquids***

The acoustic attenuation coefficient inside a liquid, $\alpha$, is very often assumed to have three contributions[48]. A first contribution is connected with the dynamical (or shear) viscosity $\mu$, a second contribution is related to the bulk viscosity $\eta$, and a final contribution takes into account thermal effects. The expression proposed by Nash *et al.* [48] is:

$$N = \frac{\alpha}{f^2} = \frac{2\pi^2}{\rho c^3}\left(\frac{4}{3}\mu + \eta + \frac{c^2\beta^2\lambda T}{C_p^2}\right) \tag{15}$$

where $f$ is the frequency, $\rho$ is the density, $c$ is the wave velocity, $\beta$ is the thermal expansion coefficient, $\lambda$ is the thermal conductivity, $C_p$ is the specific heat, and $T$ is the absolute temperature. The dynamical viscosity $\mu$ and the properties involved in the thermal contribution can generally be obtained for standard liquids with an acceptable accuracy, so that the main difficulty will come from the estimation of the bulk viscosity $\eta$. For example, even for a fluid as studied as water, various estimations of $\eta$ can be found in the literature[42,49], from which different values of the acoustic attenuation coefficient can be obtained. We have summarized the estimations of the different contributions to the acoustic attenuation coefficient for water in each of these cases in table 1 (the values of the properties used for water at 20°C are $\rho$ = 998.2 Kg/m$^3$, $\beta$ = 2.07 10$^{-4}$ K$^{-1}$, $C_p$ = 4180 J K$^{-1}$kg$^{-1}$, $c$ =1480 m/s, $\lambda$ = 0.61 W.m$^{-1}$K$^{-1}$, $\mu$ = 0.001 Pa.s). In table 1, the first column represents an hypothetical water where the bulk viscosity term can be neglected (Stokes hypothesis). We see that for such hypothetical fluid the term connected with thermal effects is small; hence it is commonly neglected, as done here in the three other columns. The term associated to the dynamical

viscosity is assumed to be well known, so that the main uncertainty comes from the bulk viscosity which, according to existing litterature[47,49,51] is not at all negligible for water. The acoustic attenuation coefficient can thus vary, for a 2 MHz wave in water, from 0.03 if we neglect the bulk viscosity term (Stokes hypothesis) to 0.083, 0.09 and 0.105 $m^{-1}$, depending on the value of the bulk viscosity according to literature. The estimation of $\eta$ given by Kinsler *et al.*[42] seems reasonable as it allows finding a value of $N$ close to the measured value, which is reported in the Kaye and Laby Tables[50] to be $N = \alpha/f^2 = 250.10^{-16}\ s^2/m$ for water at 20°C. We use this measured value in the following. The corresponding values of the attenuation coefficient are typically $\alpha = 0.1\ m^{-1}$ for $f = 2$ MHz and $\alpha = 0.625\ m^{-1}$ for $f = 5$ MHz.

| **Water at 20°C** | **Water (Stokes hypothesis)** | **Water**[49] | **Water**[51] | **Water**[42] |
|---|---|---|---|---|
| Term connected with the bulk viscosity, $\eta$ (mPa.s) | 0 | 2.1 $\mu$ = 2.1 | 2.4 $\mu$ = 2.4 | 3 $\mu$ =3 |
| Term connected with the dynamical viscosity, 4/3$\mu$ (mPa.s) | 1.33 | 1.33 | 1.33 | 1.33 |
| Term connected with thermal effects (mPa.s) | 0.96 $10^{-3}$ | Neglected | Neglected | Neglected |
| Prefactor $\frac{2\pi^2}{\rho c^3}$ (s/mPa.m) | 60.63 $10^{-16}$ | 60.63 $10^{-16}$ | 60.63 $10^{-16}$ | 60.63 $10^{-16}$ |
| $\alpha/f^2$ ($s^2/m$) | 80.9 $10^{-16}$ | 208 $10^{-16}$ | 226 $10^{-16}$ | 263 $10^{-16}$ |
| $\alpha$ ($m^{-1}$) for $f$ = 2 MHz | 0.032 | 0.083 | 0.090 | 0.105 |
| $\alpha$ ($m^{-1}$) for $f$ = 5 MHz | 0.202 | 0.52 | 0.565 | 0.66 |

**Table 1: Estimations of the different contributions to the acoustic attenuation coefficient in water.**

## *3. Scaling Analysis.*

### *Order of magnitude of acoustic streaming flow velocities*

In this section we consider a steady, laminar, acoustic streaming jet in a semi-infinite medium. Under these conditions, the pressure gradient does not play any significant role. The flow is thus governed by a balance between the combined effects of viscosity, inertia and the acoustic streaming force. We focus successively on the two asymptotic cases of negligible viscous effects and negligible inertia effects.

***Inertia dominated regime near the origin of the jet.***

Let us first consider the acceleration zone near the origin of the jet where inertia plays an important role. The balance between inertial terms and acoustic force can be written, in an order of magnitude sense, on the beam axis:

$$\rho \frac{\partial u^2}{\partial x} \propto \frac{2\alpha I_{ac}}{c}. \tag{16}$$

The overall power of the beam, $P_{ac}$, is given by:

$$P_{ac} = \int_0^{R_{beam}} I_{ac}(r)\, 2\pi\, r dr, \tag{17}$$

where $R_{beam}$ is the radius of the acoustic beam. Still from an order of magnitude perspective, one can thus write :

$$I_{ac} \propto \frac{P_{ac}}{\pi R_{beam}^2}. \tag{18}$$

From equation (16), the typical velocity $u$ at a distance $x$ from the origin of the jet is then expected to follow the following scaling law:

$$u \propto \sqrt{\frac{2\alpha}{\rho c}\frac{P_{ac}}{\pi R_{beam}^2} x} \quad \text{be} \quad u \approx \kappa_1 \sqrt{\frac{2\alpha}{\rho c}\frac{P_{ac}}{\pi R_{beam}^2} x}\ , \tag{19}$$

where $\kappa_1$ is a multiplicative factor of the order of 1. At this stage let us just mention that such a scaling with the acoustic power root is rarely mentioned in the literature, but has been observed in an experimental work by Mitome *et al.* [38].

***Viscosity dominated regime far from the origin of the jet.***

Further from the origin, the longitudinal velocity variations can be expected to be weaker so that the occurrence of a flow ruled by the balance between the acoustic force and viscous forces is possible. Assuming the flow is laminar and nearly one-dimensional, the balance between streaming volumetric forces and viscous forces, can be written in an order of magnitude sense:

$$\frac{2\alpha I_{ac}}{c} \propto \mu \frac{u}{R_{jet}^2}, \tag{20}$$

in which the acoustic power can again be introduced using equation (18), which gives:

$$\frac{2\alpha}{c}\frac{P_{ac}}{\pi R_{beam}^2} \propto \mu \frac{u_{\max}}{R_{jet}^2}. \tag{21}$$

An order of magnitude of the velocity $u$ can be obtained assuming that the jet has nearly the same radius than the beam *i.e.* $R_{jet} \approx R_{beam}$. Solving equation (21) for $u$ gives then:

$$u \propto \frac{\alpha P_{ac}}{\pi \mu c} \quad \text{be} \quad u \approx \kappa_2 \frac{\alpha P_{ac}}{\pi \mu c}, \tag{22}$$

where $\kappa_2$ is a multiplicative factor of the order of 1.

The proportionality of the obtained velocity with the acoustic power is often reported in the literature. In particular this scaling is claimed to be observed experimentally by Frenkel *et al.*[4], Nowicki *et al.*[39,40] and Mitome[38]. A deeper discussion about these observations is proposed in the next section of the present paper.

This last discussion underscores the fact that the cross-section of the jet has not compulsorily the same size than that of the beam, as assumed to derive equation (22). In particular, in a semi-infinite domain, two mechanisms can be expected to drive the longitudinal evolution of the jet and the beam: viscous diffusion and diffraction, respectively. The question to answer is thus: why would the jet cross section scale with the acoustic beam cross section when it is free to do so? Scaling analysis can give clues to answer this question. To start with, we know that diffraction leads to the enlargement of the acoustic beam along the $x$ direction. For small angle, we can approximate the angle by its tangent; the acoustic beam is then found to increase in diameter at the rate:

$$\frac{\delta R_{diffraction}}{x} = 1.22\frac{\lambda}{D_s}. \tag{23}$$

This radial growth of the force field, *i.e.* of the beam size, can be compared to the enlargement law of a laminar jet by viscous diffusion according to the following scaling law[52,53]:

$$\frac{\delta R_{diffusion}}{x} = \sqrt{\frac{\nu}{u(x)x}} = \mathrm{Re}_x^{-1/2}. \tag{24}$$

Comparing diffraction and diffusion enlargement rate, we obtain:

$$\frac{\delta R_{diffraction}}{\delta R_{diffusion}} = 1.22\frac{\lambda}{D_s}\mathrm{Re}_x^{1/2}. \tag{25}$$

This ratio is proportional to the square root of the distance from the wall, $x$. Close to the jet origin, the transverse growth is due to viscous diffusion whereas far from there it is driven by diffraction in the acoustic (force) field. Introducing expression (22) in equation (25), we find the distance after which the jet is governed by diffraction:

$$\frac{x_{\lim}}{L_f} = \frac{8\pi}{1.22^2}\frac{\mu^2 f}{\alpha\rho P_{ac}} \tag{26}$$

Note that, increasing the acoustic power leads to a decrease in $x_{lim}$. Equation (26) can be seen as giving an estimate of how long the domain of investigation must be for the order of magnitude given by equation (22) to be observed in the acoustic far field.

## *4. Comparison with experimental data.*

### *Brief description of our experimental setup.*

We have designed a setup dedicated to the characterization of an acoustic streaming flow, which will be briefly presented here; the interested reader is referred to a former publication[35] for a more detailed description. As shown in figure 1, a 2MHz ultrasonic circular plane transducer, with effective diameter $D_s$ = 28.5 mm, is placed in an aquarium filled with water.

Assuming the sound velocity in water to be $c$ = 1480 *m/s*, the Fresnel length value is $L_f$ = 274 mm. Two acoustically absorbing plates are introduced. The first plate is put along the wall at the end of the cavity to avoid reflected waves (on the right of the figure). The second plate is drilled with a hole which is covered with a plastic film. This plastic film is seen as a rigid wall for the hydrodynamic problem while it lets the acoustic waves enter the domain of investigation on the right of the figure. Setting this wall at the position corresponding to the Fresnel length makes it possible to investigate the acoustic streaming flow driven by the acoustic far field in a rectangular cavity. The hole diameter is about twice the transducer diameter. Inner dimensions of the domain of investigation are 16 cm x 18 cm x 47cm (depth x width x length). The acoustic field is characterized *via* pressure measurements. A three dimensional motorized system is used to move a 1mm diameter needle hydrophone from Precision acoustics™ in order to map the acoustic pressure field in the horizontal middle plane (see figure 2). We use the *Labview*™ software through a PXI unit from *National Instruments*™ to supply the transducer *via* a power-amplifier and a wattmeter, to acquire voltage on hydrophone terminals and to control the motorized system motion. The wattmeter allows us to read the incident electrical power sent to the transducer; this power is regulated to stay constant all along the experiment. The acoustic streaming flow is characterized by Particle Image Velocimetry measurements (PIV) thanks to another independent system. The two characterizations cannot be made simultaneously since the hydrophone and its holder are intrusive; they are removed before carrying out PIV sessions. We formerly took care to check that the measured velocity field is independent of the seeding[35] (here, 5 μm diameter PSP particles from *Dantec dynamics*™).

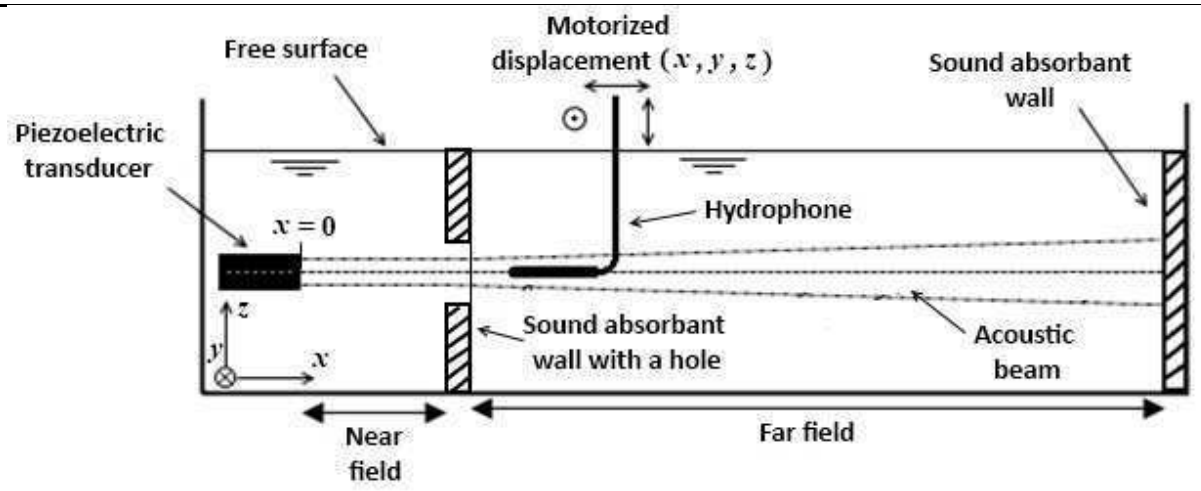


**Figure 1: Experimental configuration (side view); the sound-absorbing wall with the hole is covered with a plastic film to impose a no-slip boundary condition for the hydrodynamic flow. The origin of the frame is chosen at the center of this hole .The domain of investigation, situated on the right hand side of the absorbing wall with a hole ($x$ >0) is 16 cm deep, 18 cm wide and 47 cm long.**

A typical acoustic pressure amplitude map in the horizontal middle plane of the fluid domain is plotted in figure 2. To clearly show the near field/far field structure, the absorbing drilled wall has been removed from its location at $x = 0$; this location is however represented by a vertical dash-line. The acoustic source is set at $x$ = -275 mm, *i.e.* $x \approx - L_f$. It has been verified that introducing this wall induces negligible changes in the acoustic field in the investigation area ($x$ > 0). The diffraction cone is clearly visible on this picture. Mind that the scale is very

different on the ***y***-axis and on the ***x***-axis of this plot so that the represented region is in fact very elongated.

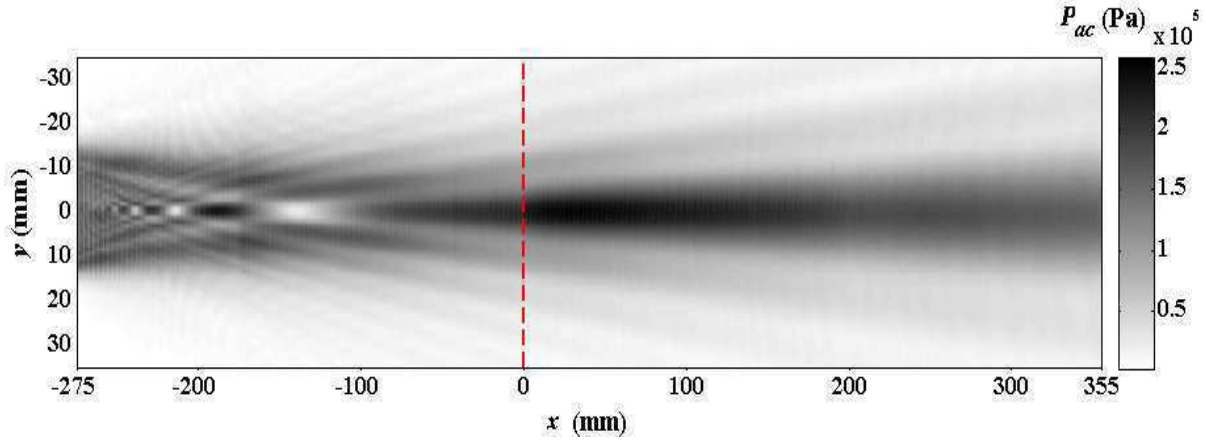


**Figure 2: Experimental map of acoustic pressure amplitude in the horizontal middle plane *(xy)*. The measurement has been made in three separate runs. The acoustic source is situated at $x \approx -L_f$. These measurements have been performed without the acoustically transmitting wall otherwise situated at $x = 0$ and represented here by a vertical dash-line. This last has been removed to show the near/far field structure. Note that the scale is very different on the *y*-axis and on the *x*-axis, so that this figure represents in fact a very elongated region.**

### *Shape of the jet vs shape of the beam.*

Experimental acoustic intensity profiles and axial velocity profiles in the middle horizontal plane are plotted together in figure 3 at $x=0.5L_f$, $x=1L_f$ and $x=1.3L_f$ . The profiles are normalized so that they reach the same value at $y/D_s = 0$; their shape can then be compared at a glance.

Clearly, the shape of the three velocity profiles is closely linked to that of the intensity profiles. The dashed straight lines correspond to the diffraction cone, given by equation (14); these lines are seen to roughly correspond to the first local minimum in the acoustic intensity profiles, as expected from the theory. One can notice that this minimum is not a zero. Let us recall that the analytical expression for the intensity profile featuring a Cardinal-Bessel function with zero at this point[37] is valid in the asymptotically far field only. Here the minimum is non-zero since the measurements are not located far enough from the source for this asymptotic case to be reached. The enlargement of the beam can be observed on the acoustic intensity profiles, plotted with dots: using the dashed lines to define a measure of the diameter, we find 24 mm at $x/L_f = 0.5$, 34 mm at $x/L_f = 2$ and 40 mm at $x/L_f = 1.3$. The transverse velocity profiles plotted as black lines were obtained for an acoustic power of 2.8W. Looking very carefully, a slight bending in their shape even seems to be present at the level of the secondary local maxima in acoustic intensity. Vertical solid lines represent both the locations where profiles are taken in the aquarium and the zero value for acoustic and velocity quantities.

This picture clearly supports the assumption made to derive equation (22), namely that the diameters of the jet and of the beam have similar values. Note that, as in figure 2, the represented region is a very elongated one, since $L_f = D_s^2/\lambda >> D_s$ in our experiment. It is also consistent with the scaling analysis of section 3. Since equation (26) predicts that the jet shape could follow the beam shape after a few centimeters only: here $x_{lim}/L_f = 0.13$, be $x_{lim} = 3.7$ cm. This behavior shows that accounting for diffraction is a key ingredient in the modeling of

acoustic streaming for this configuration. Note that former studies presenting transverse velocity profiles focused on its very local shape near the maximum velocity and maximum acoustic intensity[54,55] so that no conclusion can be drawn on this point from these papers. Specific mention must be made of the work by Kamakura *et al.*[36] which shows similar results concerning the correlation of velocity and acoustic intensity profiles in the near-field region.

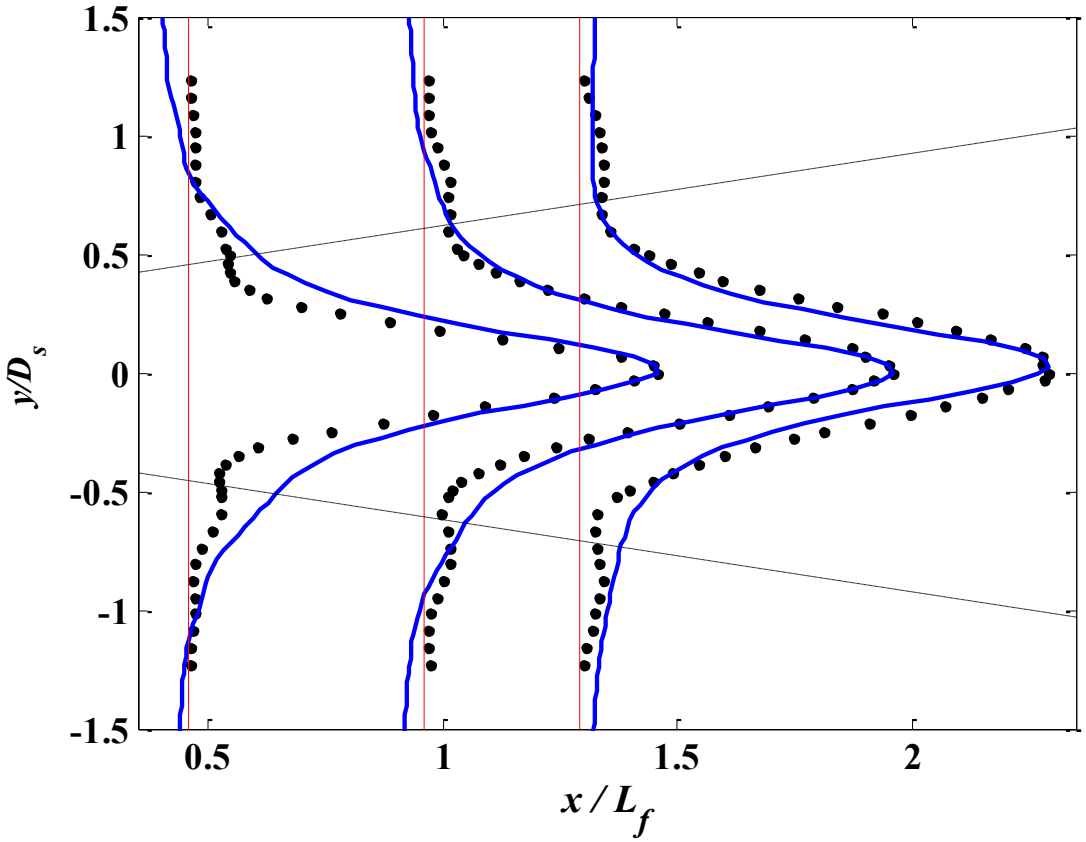


**Figure 3: Experimental profiles of normalized acoustic intensity (dots) and normalized axial velocity (solid blue lines) along the *y* axis at $x = 0.5L_f$, $x = L_f$ and at $x = 1.3L_f$ for an acoustical power of 2.8W. The two dash-dotted lines correspond to the diffraction cone (equation (14)). Note that the scale is very different on the *y*-axis and on the *x*-axis, so that this figure represents in fact a very elongated region, since $L_f = D_s^2/\lambda >> D_s$ in our experiment.**

### *Confrontation of scaling arguments with present and former experimental data.*

Previous velocity measurements of acoustic streaming driven by plane ultrasonic sources in large cavities differ in particular by the size of the source and of the set-up and by the frequency of the ultrasounds used[4,36,38–40]. The frequency varies from 2MHz in the present study to 32 MHz in the experiments by Nowicki *et al.*[39,40]. As the attenuation coefficient of sound in water is proportional to the squared frequency, its values are expected to vary by more than two decades between these studies. Conversely, the maximum power used in these investigations ranges from 0.6 mW to 10 W, that is more than three decades in power. This offers a good opportunity to check the scaling laws given in section 3. A summary of the experimental conditions in these five investigations, along with those in our own present

work, is shown in table 3. These investigations all involve circular plane transducers emitting continuous waves. The main experimental parameters are recalled in table 3; the Fresnel length and the estimated attenuation coefficient are also indicated. Comparing the Fresnel length to the length of the tank and the location of the measurement point, it can be inferred that some of these measurements are made in the near acoustic field.

| | Nowicki*et al*[39,40] | Mitome[38] | Frenkel*et al*[4] | Present study | Kamakura*et al*[36] |
|---|---|---|---|---|---|
| Rectangular cavity dimensions (depth x width x length) (cm) | 6.4 x 6.4 x 9 | 36 x 30 x60 | 25 x 17 x 14 | 18 x 16 x 47 | Cylinder 4.3cm radius 27cm length |
| Fluid | Water | Water | Water | Water | Water |
| Source Diameter $D_s$ (cm) | 0.8 | 1 | 2.52 | 2.85 | 0.9 |
| Frequency $f$ (MHz) | 32 | 5.05 | 3 | 2 | 5 |
| Attenuation $\alpha$ ($m^{-1}$) $\alpha = N f^2$ with $N = 25.10^{-15} m^{-1} s^2$ | 25.6 | 0.637 | 0.225 | 0.1 | 0.57 |
| $L_f$ (cm) from equation (13) | 34.6 | 8.53 | 32 | 27.4 | 27.4 |
| Distance $x$ from the transducer to the measurement point or area (cm) | 0 to 1.5 cm 0 to $0.04L_f$ | 0 to 20 cm 0 to $2.3L_f$ | ~3cm $\approx 0.09L_f$ | $Lf$ to 3 $Lf$ | 0 to $Lf$ |
| Investigated acoustic power range (assuming 100% efficiency) (W) | $6\ 10^{-4}$ to $6\ 10^{-3}$ W | $1.2\ 10^{-2}$ to 1.2 W | 2 to 10 W | 0.7 to 5.6 W | 0.68 W |

**Table 3: Main parameters in former and present experimental investigations.**

Except in Kamakura *et al.* who explicitly focus on the acoustic near-field, diffraction is not discussed in these former papers. The investigation zone is in particular not clearly situated with respect to the near to far field transition. For instance, Mitome[38] studies the establishment process of acoustic streaming with a 10 mm diameter 5.05MHz ultrasound transducer. Numerical application of equation (13), in this case, leads to a Fresnel length value of 85.3 mm. Measurement points are chosen at 20, 50, 80, 100 and 200 mm from the transducer, so both in the near field and in the far field without distinguishing the two areas. Likewise, Nowicki *et al.*[39,40] measure velocities on the axis of an 8 mm diameter transducer with a frequency of 32MHz up to a distance of 15 mm from the transducer whereas the near field length is 346 mm. Their investigation is thus restricted to a very small area in the near-field. Similarly, one can estimate that the quantitative data given by Frenkel *et al.*[4] are taken in the very acoustic near field. Finally, Kamakura *et al.*[36] explicitly investigate the flow in the near acoustic field, over the whole Fresnel length, with a particular attention to diffraction effects. As exposed here above, our investigation area begins on the contrary at the end of the near field; its length is equivalent to twice the Fresnel length. Our study can thus be seen as complementary to that by Kamakura *et al.*[36].

A test of equation (19) is plotted in figure 4: velocities measured along the beam axis in these five studies are plotted as a function of the group appearing to the power 1/2 on the right hand-side of equation (19). The values used for the evaluation of this formula are the source radius $R_{ac}$, $\mu$ = 1 mPa.s, $c$ = 1480 m/s and $\alpha = Nf^2$ with $N = 25.10^{-15}$ $m^{-1}s^2$. The data attributed to Mitome[38] are extracted from figure 2 of his paper; those attributed to Nowicki *et al.* [40] are the first seven points of the velocity profile plotted in their figure 4. The dataset from Kamakura *et al.*[36] corresponds to the first twenty centimeters of the longitudinal velocity profile plotted in their figure 6. Note that this last profile is actually obtained numerically; it is reported by these authors to be in agreement with the provided experimental data.

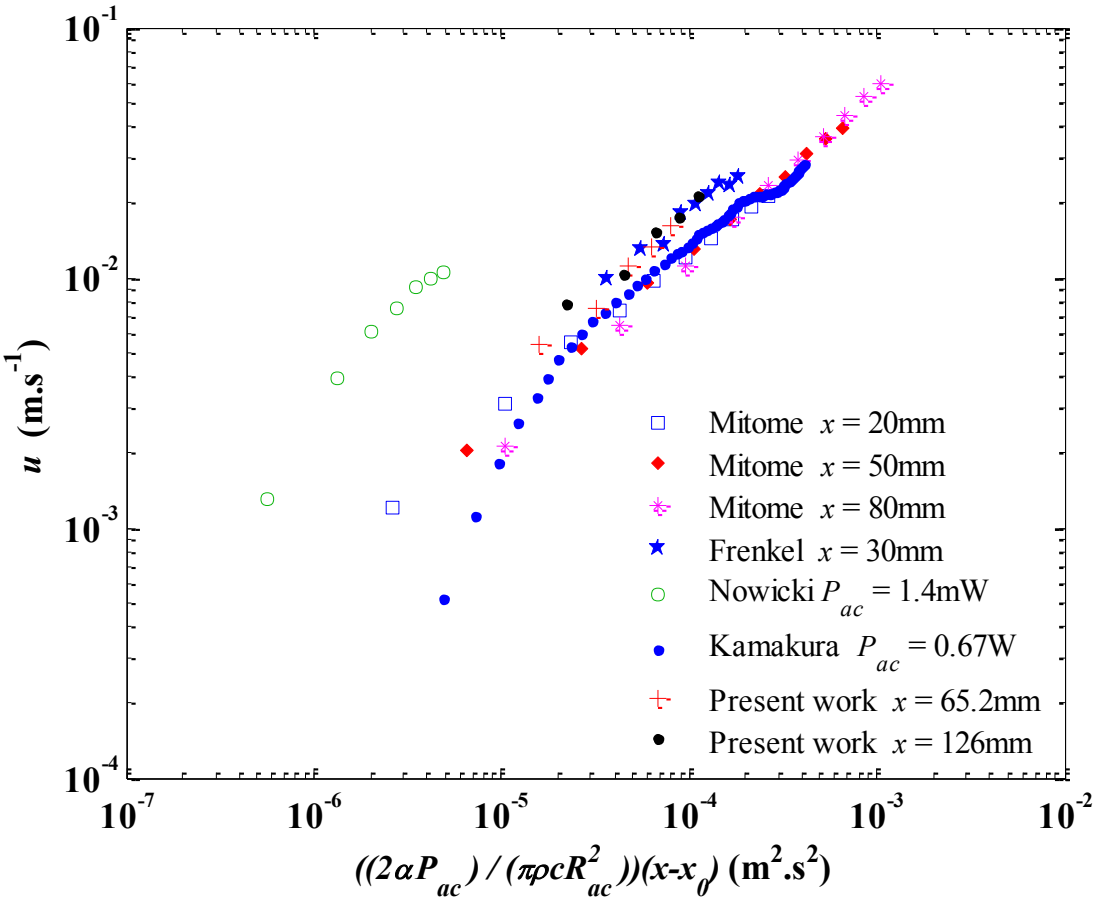


**Figure 4: Test plot of equation (19). Velocities measured in several former studies plotted as a function of the group appearing in the square root on the right hand-side of equation (19).**

This log-log plot of datasets obtained with different attenuation coefficient, source radius, power, and distance from the wall shows the occurrence of the expected power ½ behavior. Note that Kamakura *et al.* and Nowicki *et al.* provide data for a fixed value of power and varying the position, while Mitome, Frenkel *et al.* and us provide data at different value of power and fixed value of the position. A steeper slope is observed at low values for Nowicki *et al.* and Kamakura *et al.*; since these two dataset are plotted at fixed power value and varying distance from the wall, this corresponds to the very near field: typically $x/L_f < 1\%$ and 3% in the case of the data from Nowicki *et al.* and Kamakura *et al.*, respectively. This local inconsistency with the behavior expected from expression (19) may come from the great complexity of the acoustic field in this area, which is not accounted for in the derivation. The

oscillations observed at high $x$-values in Kamakura's data are due to the strong, but slower, spatial variations of the acoustic intensity along the beam axis near the end of the acoustic near-field[36,41]. As equation (18) is an order of magnitude expression, the observed values are expected to match this equation while allowing for a multiplicative factor, $\kappa_1$, of order one. This pre-factor can differ from one dataset to another, since it is expected to depend on the experimental geometry and on the location of the measurement point. The values of $\kappa_1$ obtained by a linear regression of the experimental data with respect to equation (19) are given for each dataset in the first row of table 4; the second row gives the difference between the regression and the corresponding dataset in a root mean square sense.

| | Mitome | | | Present work | | Frenkel | Kamakura | Nowicki |
|---|---|---|---|---|---|---|---|---|
| | $x$=20mm | $x$=50mm | $x$=80mm | $x$=126mm | $x$=65.2mm | $x$=30mm | | |
| Multiplicative factor $\kappa_1$ with respect to equation (19) | 1.28 | 1.48 | 1.68 | 1.85 | 1.63 | 1.85 | 1.35 | 4.53 |
| *rms* difference ($m.s^{-1}$) | $6.2\ 10^{-4}$ | $16\ 10^{-4}$ | $37\ 10^{-4}$ | $12\ 10^{-4}$ | $10\ 10^{-4}$ | $10\ 10^{-4}$ | $10\ 10^{-4}$ | $9\ 10^{-4}$ |

**Table 4: Multiplicative factor $\kappa_1$ with respect to equation (19) obtained by a linear regression of each dataset. The rms difference between the fit and the velocity data is also given (values of the velocities are on the order of $10^{-2}$ m/s)**

It must be underscored that our dataset is the only one on this plot not to be taken in the near acoustic field. The exact location where Frenkel's dataset is measured is not very clearly reported by this author, as well as the source diameter in Nowicki's work. It must also be noticed that Frenkel's data-points appear in this plot to follow a $P_{ac}^{1/2}$ behaviour, despite the fact that Frenkel presents them to be proportional to $P_{ac}$ in his figure 3. Here the *rms* difference is 0.001 $m.s^{-1}$ while it would be 0.0028 $m.s^{-1}$ assuming proportionality to $P_{ac}$ (as listed in table 5); this confirms that the $P_{ac}^{1/2}$ model better describes this data than the $P_{ac}$ model. Frenkel's data are actually taken only 1.4 diameters far from the source, which is very close to the acoustic source.

Mitome[38] presents velocity data showing proportionality with the acoustic pressure level for three distances from the transducer in figure 5 of his paper. As the acoustic power is proportional to the squared pressure, this is consistent with equation (19) as seen here in figure 4. Mitome also provides a plot of the longitudinal velocity profiles (his figure 2) as a function of the distance to the transducer, which ranges from zero to 200 mm; it must be stressed that the data used to plot his figure 5 are all taken at a distance to the transducer smaller than 50 mm. In the following, we use the velocity values from Mitome's figure 2 at points further from the source to test our second scaling law, namely equation (22).

The test for the scaling given by equation (22) is plotted in figure 5: several datasets are plotted versus the right-hand side of this equation. The experimental dataset attributed to Nowicki *et al.* [40] has been extracted from their figure 2. The values reported here for Mitome[38] are chosen 150 mm and 200 mm far from the acoustic source in their figure 2. Note that other values given every ten millimeters between these two abscissa are not reported here for the sake of clarity, but they obviously have the same behavior since this range of abscissa corresponds to a plateau in the velocity profiles.

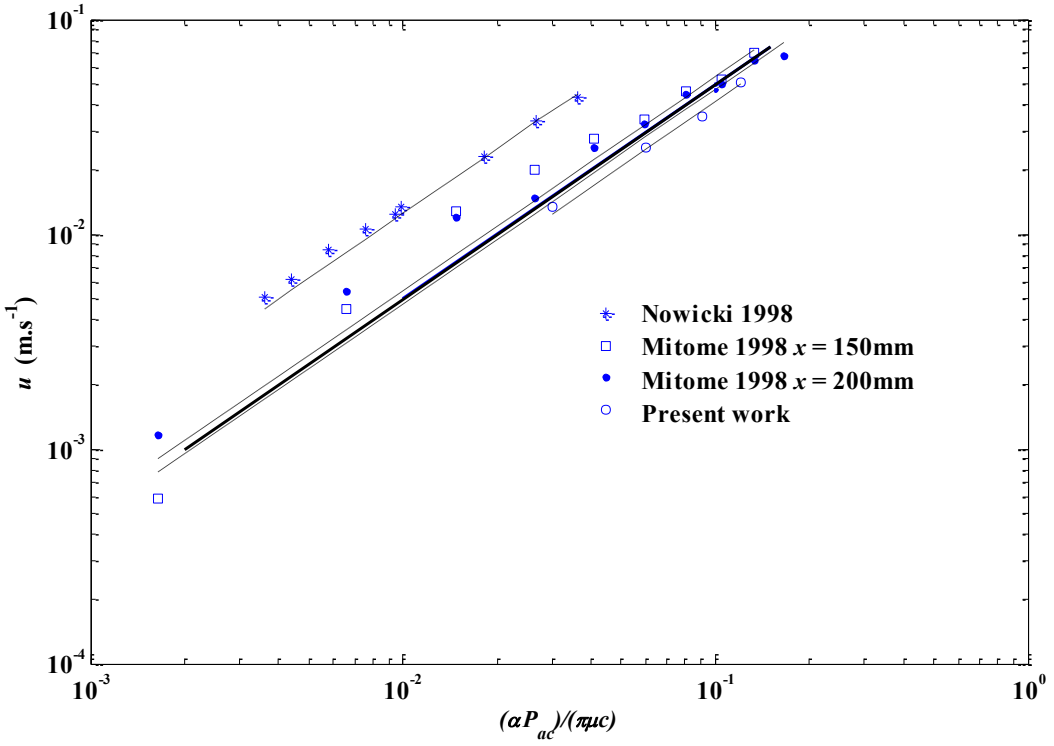


**Figure 5: Test plot of equation (22). Markers correspond to experimental measurements obtained at different powers. The full line corresponds to equation (22) arbitrarily assuming a multiplicative factor $\kappa_2$ = 1/2; the dashed-dotted black lines are obtained by linear regression to the experimental data.**

The multiplicative factor $\kappa_2$ is computed for each dataset through a linear regression and reported in table 5. One can consider that the order of magnitude given by equation (22) satisfactorily describes the datasets from Nowicki *et al.*[39,40], Mitome[38] and the present team. Indeed the plots show that the variations are nearly linear and the obtained values of $\kappa_2$ are on the order of 1. Let us recall that the assumptions for equation (22) to hold are the validity of the force expression given by equation (12), the occurrence of a viscous force dominated equilibrium, and the equality between the beam and the jet diameters. From table 3, it can be seen that for Mitome's study and ours, the datasets are taken in the far field so that the assumption concerning the diameter of the jet can be converted into a condition on the distance from the wall: it should be greater than the value $x_{lim}$ given by equation (25). The third line of table 5 gives the range of values spanned by $x_{lim}$ in the experiments, computed from the range of involved acoustic power. This is to be compared to the location of the measurement zone also given in table 5. One can see that this assumption is fulfilled in the case of our dataset. It is also fulfilled in the upper range of acoustic powers investigated by Mitome[38].

On the other hand, Nowicki *et al.*[39,40] operate in the very near field where , as far as we know, even the expression of the acoustic force in this zone is not clearly established from a theoretical standpoint. The linear behavior observed by Nowicki and the order of magnitude of the measured velocities are both found to be compatible with equation (12); in the same time, the data from Kamakura *et al.*, Frenkel *et al.* and Nowicki *et al.* plotted in figure 4, all taken in the near field, are also consistent with relation (19). This seems to indicate that equation (12) is at least a good approximation in the near field. This question should be

addressed in the future by means of numerical simulations confronted to a dedicated detailed experimental investigation of acoustic streaming flow in the near field[41].

| | Nowicki *et al.*[39,40] | Mitome[38] $x = 150mm$ | Mitome[38] $x = 200mm$ | Present study |
|---|---|---|---|---|
| Multiplicative factor with respect to equation (22) | 1.25 | 0.54 | 0.47 | 0.41 |
| *rms* difference ($m.s^{-1}$) | $0.8\ 10^{-3}$ | $3.4\ 10^{-3}$ | $4.7\ 10^{-3}$ | $1\ 10^{-3}$ |
| Range of $x_{lim}$ equation (25) in *cm* | 113 to 1126 | 1.2 to 95 | 1.2 to 95 | 1.7 to 6.6 |
| Distance to the wall (*cm*) | 0.6 | 15 | 20 | 26.8 |

**Table 5: Multiplicative factor $\kappa_2$ with respect to equation (22) obtained by a linear regression of each dataset presented in figure 5. The rms difference between the fit and the velocity data is also given (values of the velocities are on the order of $10^{-2}$ m/s). The value of the range of $x_{lim}$ from equation (26) and the distance to the wall.**

To sum things up, we have thus presented a scaling analysis giving orders of magnitude for the velocities in acoustic streaming jets. Two scaling laws are proposed depending on whether the momentum balance is dominated by viscous forces or by inertia, namely equations (22) and (19), respectively. Equation (22) requires in addition the assumption that the beam and the jet have nearly the same transverse dimension. In the acoustic far field this can be obtained in the case when the transverse growth of the acoustic beam due to diffraction is faster than the viscous diffusion induced transverse growth of the jet. The minimum distance from the origin of the jet for this assumption to hold is given by equation (26). As diffraction is a key ingredient in this analysis, our own experimental setup has been designed to account for diffraction: the near and far field can be separated by an acoustically transmitting wall and the length of the investigation area is several times the Fresnel length. The proposed scaling laws are shown to be globally consistent both with formerly published experimental data and with our proper measurements.

## *5. Dimensional analysis.*

### *Set of dimensionless parameters*

As a consequence of the former developments, we consider that a good description of an acoustic streaming free jet must necessarily feature both a description of the acoustic propagation problem, including diffraction, and a description of the incompressible fluid flow problem. Dimensional analysis necessitates first to determine the set of physical dimensional parameters implied in the observed phenomena. The Vaschy-Buckingham theorem then allows the computation of minimum number of dimensionless groups needed to describe the problem.

Let us consider that the aim of the analysis is to investigate the link between the acoustic power $P$ of the sound source and an observed typical velocity $U$. This velocity can for example be chosen as the maximum velocity in the fluid domain or alternatively the velocity at an arbitrary location in the domain. If we consider a simple geometry with a fluid domain

of square cross section of side $l$ and length $L$, the hydrodynamic problem features 5 variables: the velocity, $U$, the liquid density and kinematic viscosity, $\rho$ and $\nu$, and these two dimensions, $l$ and $L$. Five dimensional variables are required to describe the acoustic problem: the power and diameter of the plane source, respectively $P$ and $D_s$, the sound attenuation coefficient $\alpha$, as well as the frequency and celerity of the wave, respectively, $f$ and $c$. As discussed in section 3, in Newtonian fluids, the attenuation is known to be proportional to the square of the frequency[42,56]. This leads us to replace $\alpha$ in the list of parameters by $N = \alpha/f^2$; the variable $N$ is a physical property of the material; as such, in the framework of our dimensional analysis, it must be preferred to $\alpha$ which is frequency dependent. All these variables are listed in the first column of table 6, while the second column gives their usual units and the third column gives the transcription of this units in terms of the three fundamental units of mechanics, length ($m$), time ($s$) and mass ($kg$). As ten variables are thus involved in our problem and since their units can be expressed with three fundamental units only, the Vaschy-Buckingham theorem states that 10-3= 7 dimensionless groups are required to fully characterize this problem. It is well known that these numbers are not defined uniquely so that the user can choose the most convenient combination between several possibilities. The groups we have chosen are given in the fourth column of table 6. They have been obtained by choosing $D_s$, $D_s^2/\nu$ and $\rho.D_s^3$ as characteristic scales for length, time and mass respectively.

| Dimensional variables | Usual units | Fundamental units | Corresponding dimensionless group |
|---|---|---|---|
| $N = \alpha/f^2$ | $m^{-1}.Hz^{-2}$ | $m^{-1}s^2$ | $\mathbf{N}=N f^2 L$ |
| $f$ | $Hz$ | $s^{-1}$ | $\mathbf{F}=fD_s^2/\nu$ |
| $\lambda=c/f$ | $m$ | $M$ | $\mathbf{S} = 1.22\lambda/D_s$ |
| $L,l$ and $D_s$ | $m$ | $M$ | $\mathbf{L}=L/D_s$, $\mathbf{l} = l/D_s$ |
| $P$ | $W$ | $kg.m^2s^{-3}$ | $\mathbf{P} = P.D_s/(\rho.\nu^3)$ |
| $U$ | $m.s^{-1}$ | $m.s^{-1}$ | $\mathbf{U}=U.D_s/\nu$ |
| $\nu$ | $m^2.s^{-1}$ | $m^2.s^{-1}$ | - |
| $\rho$ | $kg.m^{-3}$ | $kg.m^{-3}$ | - |

**Table 6: Variables of the problem, their units and the corresponding dimensionless groups.**

Each dimensionless group in this table can be associated with a physical interpretation.

**N** is a ratio between the length of the domain $L$ and the typical attenuation distance $1/\alpha$. It can give an estimate of the proportion of the acoustic power $P$ that is converted into a working force within the fluid, and also an estimate of the longitudinal decrease in acoustic intensity under the effect of sound attenuation.

**F** is the dimensionless frequency and can be seen as a ratio of the period and the characteristic time for viscous diffusion of momentum at the scale $D_s$ [57]. This number has very high values except for microfluidic values of $D_s$. Simple algebra shows that $\mathbf{F}.\pi = D_s^2/\delta^2$ (see discussion on Rayleigh-Schlichting streaming in the introduction), which indicates that acoustic boundary layers occurring in areas where the wave propagates along walls are far smaller than the length scale $D_s$.

**S** is typically the half angle of the diffraction cone of the sound beam (assuming **S** is small enough to assess $arcsin(\mathbf{S}) \sim \mathbf{S}$, see equation (14)),

**L and l** are simply the ratios of the cavity length and width to the source diameter. Any other length-scale introduced in the problem would result in an additional aspect ratio similar to

these two. This could be the case for the account of a non-strictly rectangular geometry but also to account for a focused acoustic source of given focal length.

**U**, the dimensionless velocity, is a local Reynolds number based on the observed velocity and the source diameter. Note in particular that the momentum, heat and mass transfer properties of the flow, characterized for example through the definition of a Nusselt number, a Sherwood number or even by the friction coefficient at a wall, are classically expected to be directly correlated to **U**.

**P** is the injected acoustic power normalized by a typical power dissipated by viscous effects. Indeed, the group $\rho\nu^3/D_s$ is a typical power developed by external viscous forces acting on a $D_s$-long portion of a viscous jet with diameter $D_s$ and at Reynolds number unity.

The dimensionless form of the governing equations with this set of dimensionless parameters is given in annex of the present paper.

### *Implications of the theory of physical modeling.*

The transcription of the results from a model experiment in water to experiments in other fluids can be done relying on the former analysis and on the theory of physical modeling. As an illustration, we consider hereunder the case in which a model experiment is made with water to reproduce some application featuring another liquid. This is an arbitrary choice since one could consider, for example, a given scale to be *a priori* chosen for the model; the problem would then be to choose the appropriate model fluid. One of our concerns is also to give an estimate of what characteristic size, power, *etc* would have an application that would be similar to our setup but operating liquid metals. The relations proposed in the following are still valid without loss of generality. If we consider that the test case (the model experiment in water) is at a scale $\Sigma$ with respect to the real case, then all the geometrical dimensionless groups, that is **L** and **l**, are automatically identical between the test case and reality. A full similarity then requires the other 5 dimensionless parameters to be identical too. In the following, the dimensional and non-dimensional parameters referring to the test case and to the real case will be denoted with a subscript *test* and *real*, respectively. With these notations, the scale is thus defined by:

$$\Sigma = \frac{L_{test}}{L_{real}}. \tag{27}$$

Let us introduce compact notations denoting by $R_m = m_{test}/m_{real}$ the ratio between the value of any parameter $m$ in the test case and in the real case.

Let us first consider the similarity from the linear acoustic problem standpoint. The spatial variations of the acoustic field are characterized by the three dimensionless groups **N**, **F** and **S**. Having a full acoustic similarity requires these three groups to take the same value in the test case as in the real one; the following set of equations has thus to be verified :

$$\begin{cases} \mathbf{N}_{test} / \mathbf{N}_{real} = 1 \\ \mathbf{F}_{test} / \mathbf{F}_{real} = 1 \\ \mathbf{S}_{test} / \mathbf{S}_{real} = 1 \end{cases} \quad \text{be} \quad \begin{cases} R_N R_f^2 \Sigma = 1 \\ R_f \Sigma^2 R_\nu^{-1} = 1 \\ R_c R_f^{-1} \Sigma^{-1} = 1 \end{cases} . \tag{28}$$

As we consider here the fluid couple to be fixed, for given ambient conditions, $R_\nu$, $R_c$ and $R_N$ are fixed since they depend on the two fluids properties only, while $\Sigma$ and $R_f$ relate to the experimental configurations and must be chosen for the two cases to be in similarity. Unfortunately this 3 equations system with two unknowns is over-determined and usually has no solution. A full similarity is thus generally not possible and a choice must be made to limit the acoustic similarity to two dimensionless groups at the expense of the third one. Note that in the general framework of fluid dynamics, it is rare to be able to establish a full similarity between two hydrodynamic problems (see for example the case of free surface hydraulics in which a similarity in terms of Reynolds number and Froude number is not possible in a water model experiment[58]).

As discussed above, we consider that diffraction is a key element in the modeling of acoustic streaming flows, meaning in our opinion that the dimensionless group **S** has to be conserved in the problem formulation. As mentioned above, it can be inferred from equations (13) and (14) governing the longitudinal growth of the far field acoustic beam that, in the absence of attenuation, the acoustic intensity asymptotically decreases as $\sin(\theta)/x^2$ along the beam. This can be compared to the $e^{-2\alpha x}$ intensity decrease due to attenuation. We choose to relax the similarity condition concerning the account of attenuation in the propagation problem by dropping the dimensionless group **N**. This does not mean that attenuation is neglected in the problem, but rather that we accept the attenuation occurring in the test case to be not quantitatively representative of the attenuation in the real case. The system of equations (28) is then reduced to its second and third lines, and has the following solution for the scale and the frequency ratio:

$$\Sigma = \frac{R_\nu}{R_c} \tag{29}$$

and

$$R_f = \frac{R_c^2}{R_\nu} . \tag{30}$$

Now that this solution is determined, one can compute the ratio of the dimensionless group **N** for the test case and the reality as a function of the fluids properties,

$$\frac{\mathbf{N}_{test}}{\mathbf{N}_{real}} = \frac{R_N R_c^3}{R_\nu} . \tag{31}$$

As discussed above, this ratio is not equal to unity in the general case. The difference with respect to unity can be used to quantify how restrictive was the choice made when we decided to relax the attenuation similarity in the propagation problem.

Such a choice may appear *a priori* surprising since attenuation is the origin of the coupling between acoustics and hydrodynamics and, as such, plays a very important role in our problem. To account for this coupling while the similarity for the dimensionless group **N** has been dropped out, let us replace the dimensionless power **P** by the group **NP**. The meaning of

this substitution is that, in view of streaming issues, what matters most for the hydrodynamics problem is the acoustic streaming force, which is proportional to the attenuation coefficient times the acoustic power (global standpoint) or the acoustic intensity (local standpoint). This is particularly clear in the dimensionless form of the governing equations given in annex of the present paper (see equations (35) and (39) to (41)). A meaningful similarity is then obtained for $\mathbf{N}_{test}\mathbf{P}_{test} = \mathbf{N}_{real}\mathbf{P}_{real}$ which yields:

$$R_P = \frac{R_\rho R_\nu^3}{R_N R_c^2}. \tag{32}$$

Finally the Reynolds similarity can be written as $\mathbf{U}_{test} = \mathbf{U}_{real}$, which gives the following ratio between test case velocity and real case velocity:

$$R_U = \frac{R_\nu}{\Sigma} = R_c. \tag{33}$$

One can notice that this last relation is equivalent to a Mach similarity in which the Mach number is defined as $\mathbf{M} = U/c$. We preferably use the Reynolds number to the Mach number since the generated flow is incompressible and its transport properties (Nusselt number, Sherwood number, *etc.*) are expected to be directly correlated to the Reynolds number.

It is thus in principle possible to perform model experiments in similarity with a real case, assuming that the attenuation of sound only intervenes in coupling with the acoustic power in the fluid flow problem, which seems to be a reasonable assumption. The next section is devoted to applying this approach to the specific case of the design of a water experiment dedicated to the modeling of liquid metal setups. Another concern of this section will be to draw some conclusion concerning acoustic streaming in liquid metals from existing water experiments (such as those cited above).

## *6. Examples of application to selected liquid metals.*

The particular cases of liquid silicon and liquid sodium are considered, which makes sense in the general framework of electric energy production and of fundamental investigations in planetary and earth sciences. Liquid silicon is involved in crystal growth processes for solar-cells production, in which stirring by acoustic streaming could be of interest. Liquid sodium is used in nuclear plants design[13,18] and in academic experiments concerning the earth and planetary dynamo effect, applications that often involve ultrasonic velocimetry[14–16]. Other liquid metals or alloys could of course be of interest[17,21–23,59]; we will here focus mainly on Si and Na, which, with their very different melting point and density, are representative of the behaviors that can be met with many metallic liquids. Iron will also be considered as a reference liquid metal that is better documented. The section can also be seen as giving guidelines to assess acoustic streaming flows in any Newtonian fluid.

### *Estimation of the acoustic attenuation coefficient for a selection of liquids.*

One of the difficulties when extrapolating experimental results obtained in water to other fluids is to find the properties of the concerned fluids. In particular the acoustic attenuation

coefficient is often poorly documented. We propose hereunder a short review based on equation (15), which expresses the attenuation coefficient in terms of the mechanical and thermo-physical properties of the liquid. This leads to estimates of the attenuation coefficient in liquid silicon and liquid sodium.

For liquid iron, silicon and sodium, the values of the properties that are useful for the estimation of the acoustic attenuation coefficient are given in Table 6. The values for iron have been obtained from Nash *et al.*[56], the values for silicon from different authors[60–63], and the values for sodium from Sobolev[64]. We see that the main values are available, except the bulk viscosity for silicon and sodium. Note, however, that an expression is proposed for iron, $\eta = (3/5)\mu$, which will be used as a first approximation for silicon.

| **Property** | **Iron at 1809 K**[56] | **Silicon at 1700 K** | **Sodium at 393K** [64] |
|---|---|---|---|
| Specific heat $C_P$ (J $K^{-1}kg^{-1}$) | 748.5 | 1000 [65] | 1374 |
| Thermal conductivity $\lambda$ ($W.m^{-1}K^{-1}$) | 32.2 | 60 [60] | 85.5 |
| Thermal expansion $\beta$ ($K^{-1}$) | $0.82\ 10^{-4}$ | $1.1\ 10^{-4}$ [60] | $2.55\ 10^{-4}$ |
| Sound celerity $c$ (m/s) | 3900 | 3900 [61] | 2514 |
| Density $\rho$ ($Kg/m^3$) | 6980 | 2500 [60] | 922 |
| $\mu$ (mPa.s) | 5 | 0.8 [62] | 0.62 |
| $\eta$ (mPa.s) | $3/5.\mu = 3$ | - | - |

**Table 6: Property values useful for the estimation of the acoustic attenuation coefficient in liquid iron, silicon and sodium. Ref. : Nasch *et al.*[56], Okhotin *et al.* [65], Inatomi *et al.*[60], Hayashi *et al.*[61], Rhim and Oshaka[62], Sobolev[64] .**

We can now estimate the different contributions to the acoustic attenuation coefficient for iron, silicon and sodium. These estimations are given in table 7. We see that for these liquid metals the thermal contribution is very large and in any case much stronger than the contribution connected with the dynamical viscosity, particularly for silicon where the ratio is close to 17. Concerning the bulk viscosity, we see that it is of the same order as the dynamical viscosity for iron (factor 0.6), whereas it was a little larger (factor 3) for water. For silicon, in view of the small value of $\mu$, the contribution of the bulk viscosity can be expected to remain small and, in any case, far smaller than the thermal contribution. This contribution could have been neglected, but we chose to deduce it from the relationship between $\eta$ and $\mu$ used for iron. The values of the acoustic attenuation coefficient thus obtained for silicon ($\alpha$ = 0.01 for a 2 MHz wave) are larger than those for iron ($\alpha$ = 0.004 for a 2 MHz wave) due to the larger thermal contribution, but they are small compared to the values found for water, about ten times smaller. For sodium, the thermal contribution is still dominant, and we choose to approximate the bulk viscosity by $\eta = 1.25\ \mu$, so that the value of $\alpha/f^2$ is close to the

measured value found in the Kaye and Laby online tables[50] for sodium at 383 K ($\alpha/f^2$ =120 $10^{-16}$ $s^2/m$). The values of the acoustic attenuation coefficient obtained for sodium are then significantly larger than for the two other liquid metals, and closer to the values for water (about half the values for water).

| **About 20°C above melting temperature** | **Iron**[56] | **Silicon** | **Sodium** |
|---|---|---|---|
| Term connected with the bulk viscosity, $\eta$ (mPa.s) | 0.6 $\mu$ =3 | Approximated by<br>0.6 $\mu$ =0.48 | Approximated by<br>1.25 $\mu$ =0.77 |
| Term connected with the dynamical viscosity, 4/3 $\mu$ (mPa.s) | 6.66 | 1.07 | 0.825 |
| Term connected with thermal effects (mPa.s) | 10.62 | 18.15 | 7.3 |
| Prefactor $\frac{2\pi^2}{\rho c^3}$ (s/mPa.m) | 0.476 $10^{-16}$ | 1.33 $10^{-16}$ | 13.5 $10^{-16}$ |
| $\alpha/f^2$ ($s^2/m$) | 9.65 $10^{-16}$ | 26.2 $10^{-16}$ | 120 $10^{-16}$ |
| $\alpha$ ($m^{-1}$) for $f$ = 2MHz<br>$\alpha$ ($m^{-1}$) for $f$ = 5MHz | 0.004<br>0.024 | 0.01<br>0.065 | 0.048<br>0.3 |

**Table 7: Estimations of the acoustic attenuation coefficient in liquid iron, silicon and sodium close above the melting temperature.**

### *Implications for experimental works.*

Table 8 gives the numerical evaluation of equations (29) to (33) in the case of liquid silicon and sodium a few degrees above their respective melting points. As liquid metals exhibit both lower viscosities and higher sound celerities than water, a water model should be bigger than the setup it represents; the scale given in the first column of table 8 shows that the model must be more than eight times bigger in the case of silicon, while it is nearly twice bigger in the case of sodium. Note that this means that a water experiment must be 550 times bigger in volume than its silicon counterpart, which might be prohibitive, and only 6.8 times of its sodium counterpart. Another way to say this is that the sonicated volume in a given water experiment represents a far smaller volume in the similar case with silicon. For the same reasons, the frequency used in the water model should always be smaller than in the liquid metal application; while the ratio is between one fourth and one fifth for liquid sodium, it is less than one over twenty for liquid silicon. Let us recall that the ratio $\mathbf{N}_{test}/\mathbf{N}_{real}$ in the third column should be one for the similarity in term of attenuation to be respected. Here again the case of the sodium-water similarity is the most favorable. A water model cannot accurately

reproduce a problem with liquid silicon in which attenuation would significantly influence the spatial repartition of acoustic energy.

| | Scale $\boldsymbol{\Sigma}$ from equation (29) | $f_{test}/f_{real}$ equation (30) | $\mathbf{N}_{test}/\mathbf{N}_{real}$ equation (31) | $P_{test}/P_{real}$ equation (32) | $U_{test}/U_{real}$ equation (33) |
|---|---|---|---|---|---|
| Silicon (1750 K) | 8.2 | 0.046 | 0.17 | 8.9 | 0.38 |
| Sodium (393 K) | 2.5 | 0.23 | 0.28 | 4.9 | 0.59 |

**Table 8: Scale and the ratio of the main parameters for a model experiment in water in similarity with test cases featuring silicon and sodium (respectively first and second line).**

The power-ratio given in the fourth column can be seen as the ratio in acoustic powers to reach the same Reynolds number in water and in the liquid metal. It is greater than one in both cases; however, it is nearly identical to the scale for the silicon/water couple while it is twice the scale for the sodium/water couple. Let us remark that this ratio is very sensitive to the ratio of the viscosities in the two fluids, which appears with a power three in equation (32). One can see that the required power to reach a given Reynolds number in liquid silicon is nearly one tenth of what it is in water, a quite remarkable feature in terms of potential applications. In many applications, the Reynolds number is indeed the appropriate dimensionless number to characterize the effect of convection, since heat and mass transfer properties of the flow (characterized for example by the Nusselt and Sherwood numbers respectively) are directly correlated to it. In the case of velocimetry, what matters is rather the dimensional velocity potentially induced by the acoustic streaming. In our setup ($D_s$ = 28.5 mm, $f$ = 2 MHz), one watt of acoustic power produces a streaming velocity on the order of 1 cm/s in water (which can be retrieved as an application of equation (22)). Using this starting point, the second line of table 8 shows that, in liquid sodium, a plane transducer of diameter 12 mm operating at 8.6 MHz would induce velocities on the order of 1.7 cm/s with an acoustic power of only 200 mW. Because of the scale $\boldsymbol{\Sigma}$, we can also say that these velocities would be obtained after a smaller distance. As mentioned earlier, this numerical application makes us think that it should be taken care of acoustic streaming side-effects in ADV measurements.

## *7. Conclusion.*

The present paper focuses on acoustic streaming free jets. This is to say that progressive acoustic waves are used to generate a steady flow in the bulk of a liquid. In particular no acoustic boundary layer is present in the problem since the acoustic beam does not interact with lateral walls.

The derivation of governing equations under the form of a non-linear hydrodynamics problem coupled with an acoustic propagation problem is revisited. To do so, a time scale discrimination approach is preferred to the usually invoked amplitude perturbations expansion. Though the obtained expression for the source term in the Navier-Stokes equations is the same, this original approach provides a consistent framework with the experimental observations of acoustic streaming flows that can feature hydrodynamic non-linearities and turbulence.

A scaling analysis is performed on the basis of these equations of motion including the acoustic force. Two scaling laws are proposed for the velocity level observed on the acoustic

beam axis, depending on the most significant term considered as balancing the acoustic streaming force in the steady state momentum budget. Considering inertia, which corresponds to the acceleration zone near the origin of the jet, the velocity is expected to scale as the square root of both the acoustic power and the distance from the wall, $x$. When considering viscous effects, the velocity is expected to vary linearly with the power and to be nearly independent of $x$. In the acoustic far field, this regime is expected if the jet thickening by viscous diffusion is slower than the beam thickening by diffraction, which should be observed in long enough apparatus.

Experimental results are also presented together with a review of former experimental investigations concerning the power-to-velocity relationship for plane ultrasonic transducers in water. Our experimental study is focused on the flow in the far field, which is in particular complementary to that of Kamakura *et al.*[36] which was restricted to the near field. Our apparatus is well designed to observe the correlation between the acoustic intensity and velocity fields of the acoustic streaming driven jet under the effect of acoustic diffraction. This is illustrated here by presenting normalized transverse velocity profiles plotted on the same figure as normalized acoustic intensity profiles. This comparison of the acoustic field and the velocity field in our water experiment thus confirms that diffraction is a key ingredient in the problem. This is an important conclusion since this aspect is rarely accounted for in the literature. The literature review is also used as a test for the two scaling laws which are both observed in our setup and in former studies by other teams. The observation of the same scaling laws in the near acoustic field seems to indicate that the expression of the force established in the acoustic far field, namely equation (12), is also valid at least in an order of magnitude sense in the near field. This issue should be investigated by numerical means and dedicated experiments in the near future.

Experimental investigations related to acoustic streaming in the literature, including our own one, are yet limited to experiments in water. However a number of applications makes use of other Newtonian fluids, and in particular liquid metals. We thus propose a dimensional analysis of this problem. As diffraction has been shown to be a key ingredient in the problem, the dimensional analysis of this problem must include the acoustic parameters (celerity of sound, attenuation coefficient and diameter of the sound source), the geometrical parameters (aspect ratios), and the incompressible fluid flow parameters (density and viscosity). A set of seven dimensionless groups is then required to describe a typical acoustic experiment in a parallelipipedic aquarium of square cross-section; two of these are dedicated to the description of the geometry, so that for a model experiment at any scale, five dimensionless groups are to be considered. We show that a full similarity is usually not possible and that the similarity condition must be relaxed concerning one parameter. We show that it is preferable to relax the similarity with respect to sound attenuation since we consider experimental configurations *a priori* featuring liquids and relatively low frequencies in which neglecting attenuation at first order when computing the acoustic field would not be to critical. The scale of the model experiment is imposed by the acoustical properties of the two considered fluids; it is given by equation (29). The ratio in frequency, power and velocity between the model experiment and the real case is given by equations (30), (32) and (33) respectively. Equation (31) is itself a quantification of how restrictive is the relaxation of the similarity with respect to attenuation.

When willing to apply relations (29) to (33) to real cases, the need of data becomes pregnant. In particular the sound attenuation coefficient is not always known. This is in particular the case for melt silicon and sodium, which we have chosen to illustrate the case of crystal growth

applications, nuclear applications and earth and planetary science experiments. It was however necessary to rely on the knowledge of other physical properties to compute an estimate of the attenuation coefficient. Concerning the similarity analysis, in the case of liquid silicon, the striking result is that reaching a Reynolds number within a silicon setup requires only one tenth of the power needed to reach the same Reynolds number in the water model experiment. Such a flow would however be obtained in a far smaller sonicated volume. This part of the paper has been written with enough details to serve as guidelines for possible other studies with different liquids. In the case of liquid sodium, we show that our experimental setup may be not far from being in similarity with ultrasonic velocimetry apparatus; a numerical application shows that small powers can yield significant acoustic streaming in liquid sodium, which could yield a bias in velocimetry measurements and should better be accounted for in the future.

## *8. Acknowledgements.*

Funding for this project was provided by a grant, including a doctoral fellowship for Brahim Moudjed, from *la Région Rhône Alpes.*

## *9. Annexes.*

With the set of dimensionless parameters defined in section 5, the governing equations (7) and (8), (12), (13), (14) becomes, respectively:

$$div\mathbf{u} = 0 \quad \text{and} \quad d\mathbf{u}/d\mathbf{t} = -\vec{\nabla}\mathbf{p} + \vec{\nabla}^2\mathbf{u} + \mathbf{F}\vec{\mathbf{x}}. \tag{34}$$

with $\mathbf{t} = tD_s^2/\nu$ and $\mathbf{p} = p/\rho.D_s^3/\nu^2$. The force expressed by (13) becomes :

$$\vec{\mathbf{F}} = \mathbf{F}\vec{\mathbf{x}} = \frac{8\times 1.22}{\pi}\frac{\mathbf{NP}}{\mathbf{SFL}}\mathbf{G}(\mathbf{x},\mathbf{y},\mathbf{z})\vec{\mathbf{x}}. \tag{35}$$

where **G** is the dimensionless spatial repartition of the acoustic intensity defined by :

$$\mathbf{G} = \frac{I.\pi D_s^2/4}{P}, \tag{36}$$

Expressions (14) and (15) also give :

$$\mathbf{L_f} = \frac{L_f}{D_s} = \frac{1.22}{4\ \mathbf{S}}, \tag{37}$$

$$\sin\theta = \mathbf{S}. \tag{38}$$

Similarly, the scaling relations of section 4, respectively equations (19), (22) and (26), can be written with dimensionless variables only:

$$\mathbf{U} \propto \sqrt{\frac{8\times 1.22}{\pi}\frac{\mathbf{NP}}{\mathbf{SF}}\left(\frac{x}{L}\right)}. \tag{39}$$

$$\mathbf{U} = \frac{1.22\,\mathbf{NP}}{2\pi\,\mathbf{LSF}}\,. \tag{40}$$

$$\frac{x_{\lim}}{L_f} = \frac{8\pi}{1.22^2}\frac{\mathbf{FL}}{\mathbf{NP}} \tag{41}$$

## *10.References.*


[1] Schenker, M. C., Pourquié, M. J. B. M., Eskin, D. G. & Boersma, B. J. PIV quantification of the flow induced by an ultrasonic horn and numerical modeling of the flow and related processing times. *Ultrasonics Sonochemistry* **20,** 502–509 (2013).

[2] Aktas, M. K. & Ozgumus, T. The effects of acoustic streaming on thermal convection in an enclosure with differentially heated horizontal walls. *Int. J. Heat Mass Transf.* **53,** 5289–5297 (2010).

[3] Charrier-Mojtabi, M. C., Fontaine, A. & Mojtabi, A. Influence of acoustic streaming on thermo-diffusion in a binary mixture under microgravity. *International Journal of Heat and Mass Transfer* **55,** 5992–5999 (2012).

[4] Frenkel, V., Gurka, R., Liberzon, A., Shavit, U. & Kimmel, E. Preliminary investigations of ultrasound induced acoustic streaming using particle image velocimetry. *Ultrasonics* **39,** 153–156 (2001).

[5] Dhahbi, M., Ben Chiekh, M., Gilles, B., Béra, J. C. & Jemni, A. Numerical simulations of particle dynamics in a poststenotic blood vessel region within the scope of extracorporeal ultrasound stenosis treatment. *Medical Engineering & Physics* **34,** 982–989 (2012).

[6] Gao, D., Li, Z., Han, Q. & Zhai, Q. Effect of ultrasonic power on microstructure and mechanical properties of AZ91 alloy. *Materials Science and Engineering a-Structural Materials Properties Microstructure and Processing* **502,** 2–5 (2009).

[7] Jian, X., Xu, H., Meek, T. T. & Han, Q. Effect of power ultrasound on solidification of aluminum A356 alloy. *Materials Letters* **59,** 190–193 (2005).

[8] Jian, X., Meek, T. T. & Han, Q. Refinement of eutectic silicon phase of aluminum A356 alloy using high-intensity ultrasonic vibration. *Scripta Materialia* **54,** 893–896 (2006).

[9] Kozhemyakin, G. N. Imaging of convection in a Czochralski crucible under ultrasound waves. *Journal of Crystal Growth* **257,** 237–244 (2003).

[10] Kozhemyakin, G. Influence of Ultrasonic Vibrations on the Growth of Insb Crystals. *Journal of Crystal Growth* **149,** 266–268 (1995).

[11] Lei, Y., Hai, H., Shou-hua, J., Can-feng, F. & Xing-guo, Z. Effects of ultrasonic vibration on solidification structure and properties of Mg-8Li-3Al alloy. *Transactions of Nonferrous Metals Society of China* **21,** 1241–1246 (2011).

[12] Zhi-qiang, Z., Qi-chi, L. & Jian-zhong, C. Microstructures and mechanical properties of AZ80 alloy treated by pulsed ultrasonic vibration. *Transactions of Nonferrous Metals Society of China* **18,** S113–S116 (2008).

[13] Khadamakar, H. P., Patwardhan, A. W., Padmakumar, G. & Vaidyanathan, G. Flow distribution in the inlet plenum of steam generator. *Nuclear Engineering and Design* **241,** 4165–4180 (2011).

[14] Nataf, H.-C. *et al.* Rapidly rotating spherical Couette flow in a dipolar magnetic field: An experimental study of the mean axisymmetric flow. *Physics of the Earth and Planetary Interiors* **170,** 60–72 (2008).

[15] Brito, D. *et al.* Zonal shear and super-rotation in a magnetized spherical Couette-flow experiment. *Phys. Rev. E* **83,** (2011).

[16] Brito, D., Nataf, H.-C., Cardin, P., Aubert, J. & Masson, J.-P. Ultrasonic Doppler velocimetry in liquid gallium. *Experiments in Fluids* **31,** 653–663 (2001).
[17] Pedcenko, A., Bojarevičs, A., Priede, J., Gerbeth, G. & Hermann, R. Velocity measurements in the liquid metal flow driven by a two-phase inductor. *Exp Fluids* **54,** 1–8 (2013).
[18] Eckert, S., Buchenau, D., Gerbeth, G., Stefani, F. & Weiss, F.-P. Some Recent Developments in the Field of Measuring Techniques and Instrumentation for Liquid Metal Flows. *J. Nucl. Sci. Technol.* **48,** 490–498 (2011).
[19] Eckert, S. & Gerbeth, G. Velocity measurements in liquid sodium by means of ultrasound Doppler velocimetry. *Experiments in Fluids* **32,** 542–546 (2002).
[20] Buchenau, D., Eckert, S., Gerbeth, G., Stieglitz, R. & Dierckx, M. Measurement technique developments for LBE flows. *Journal of Nuclear Materials* **415,** 396–403 (2011).
[21] Schulenberg, T. & Stieglitz, R. Flow measurement techniques in heavy liquid metals. *Nuclear Engineering and Design* **240,** 2077–2087 (2010).
[22] Kikuchi, K., Takeda, Y., Obayashi, H., Tezuka, M. & Sato, H. Measurement of LBE flow velocity profile by UDVP. *Journal of nuclear materials* **356,** 273–279 (2006).
[23] Pothérat et al. Direct and inverse pumping in flows with homogeneous and non-homogeneous swirl. *accepted for publication in European Physical Journal* (2013).
[24] Poindexter, C. M., Rusello, P. J. & Variano, E. A. Acoustic Doppler velocimeter-induced acoustic streaming and its implications for measurement. *Exp. Fluids* **50,** 1429–1442 (2011).
[25] Barnett, S. B. *et al.* International recommendations and guidelines for the safe use of diagnostic ultrasound in medicine. *Ultrasound Med. Biol.* **26,** 355–366 (2000).
[26] Starritt, H. C. *et al.* Measurement of acoustic streaming using magnetic resonance. *Ultrasound Med. Biol.* **26,** 321–333 (2000).
[27] Zauhar, G., Starritt, H. C. & Duck, F. A. Studies of acoustic streaming in biological fluids with an ultrasound Doppler technique. *Br J Radiol* **71,** 297–302 (1998).
[28] Zauhar, G., Duck, F. A. & Starritt, H. C. Comparison of the acoustic streaming in amniotic fluid and water in medical ultrasonic beams. *Ultraschall Med.* **27,** 152–158 (2006).
[29] Schlichting, H. *Boundary Layer theory*. (MacGraw-Hill, 1955).
[30] Eckart, C. Vortices and Streams Caused by Sound Waves. *Physical Review* **73,** 68–76 (1948).
[31] Lighthill, S. J. Acoustic streaming. *J. Sound Vibr.* **61,** 391–418 (1978).
[32] Frampton, K. D., Martin, S. E. & Minor, K. The scaling of acoustic streaming for application in micro-fluidic devices. *Applied Acoustics* **64,** 681–692 (2003).
[33] Nyborg, W. L. *Acoustic streaming*. (1998).
[34] Dridi, W., Henry, D. & Ben Hadid, H. Stability of buoyant convection in a layer submitted to acoustic streaming. *Phys. Rev. E* **81,** (2010).
[35] Westervelt, P. J. The Theory of Steady Rotational Flow Generated by a Sound Field. *The Journal of the Acoustical Society of America* **25,** 60–67 (1953).
[36] Kamakura, T., Sudo, T., Matsuda, K. & Kumamoto, Y. Time evolution of acoustic streaming from a planar ultrasound source. *The Journal of the Acoustical Society of America* **100,** 132–138 (1996).
[37] Botton, V. *et al.* Etude expérimentale et théorique d'un écoulement entraîné par des ultrasons (acoustic streaming). *Actes du XX° Congrès Français de Mécanique* (2011), at http://documents.irevues.inist.fr/handle/2042/46539
[38] Mitome, H. The mechanism of generation of acoustic streaming. *Electron. Commun. Jpn. Pt. III-Fundam. Electron. Sci.* **81,** 1–8 (1998).
[39] Nowicki, A., Secomski, W. & Wojcik, J. Acoustic streaming: Comparison of low-amplitude linear model with streaming velocities measured by 32-Mhz Doppler. *Ultrasound Med. Biol.* **23,** 783–791 (1997).

[40] Nowicki, A., Kowalewski, T., Secomski, W. & Wójcik, J. Estimation of acoustical streaming: theoretical model, Doppler measurements and optical visualisation. *European Journal of Ultrasound* **7,** 73–81 (1998).
[41] Moudjed, B. Caractérisation expérimentale et théorique des écoulements entraînés par ultrasons. Perspectives d'utilisation dans les procédés de solidification du Silicium Photovoltaïque., PHD Thesis, INSA de Lyon, *in French* (2013).
[42] Kinsler, L. E., Frey, A. R., Coppens, A. B. & Sanders, J. V. *Fundamentals of acoustics*. **1,** (1999).
[43] Rudenko, O. V. & Sukhorukov, A. A. Nonstationary Eckart streaming and pumping of liquid in an ultrasonic field. *Acoust. Phys.* **44,** 565–570 (1998).
[44] Dridi, W., Henry, D. & BenHadid, H. Influence of acoustic streaming on the stability of an isothermal or laterally heated fluid layer. *C. R. Mec.* **335,** 175–180 (2007).
[45] Ben Hadid, H., Dridi, W., Botton, V., Moudjed, B. & Henry, D. Instabilities in the Rayleigh-Bénard-Eckart problem. *Phys. Rev. E* **86,** 016312 (2012).
[46] Dridi, W., Henry, D. & Ben Hadid, H. Influence of acoustic streaming on the stability of a laterally heated three-dimensional cavity (vol 77, art no 046311, 2008). *Phys. Rev. E* **77,** (2008).
[47] Dridi, W., Henry, D. & Ben Hadid, H. Influence of acoustic streaming on the stability of melt flows in horizontal Bridgman configurations. *J. Cryst. Growth* **310,** 1546–1551 (2008).
[48] Nasch, P. M., Manghnani, M. H. & Secco, R. A. A modified ultrasonic interferometer for sound velocity measurements in molten metals and alloys. *Review of Scientific Instruments* **65,** 682 –688 (1994).
[49] Pinkerton, J. M. M. The Absorption of Ultrasonic Waves in Liquids and its Relation to Molecular Constitution. *Proc. Phys. Soc. B* **62,** 129 (1949).
[50] National Physical Laboratory. Kaye and Laby Tables for Physical and Chemical Constants. at <http://www.kayelaby.npl.co.uk/>
[51] Liebermann, L. N. The second viscosity of liquids. *Physical Review* **75,** 1415 (1949).
[52] Guyon, E., Hulin, J.-P., Petit, L. & de Gennes, P. G. *Hydrodynamique physique, 2001*.
[53] Guyon, E. *Physical hydrodynamics*. (Oxford University Press, 2001).
[54] Hariharan, P. *et al.* Characterization of high intensity focused ultrasound transducers using acoustic streaming. *J. Acoust. Soc. Am.* **123,** 1706–1719 (2008).
[55] Myers, M. R., Hariharan, P. & Banerjee, R. K. Direct methods for characterizing high-intensity focused ultrasound transducers using acoustic streaming. *J. Acoust. Soc. Am.* **124,** 1790–1802 (2008).
[56] Nasch, P., Manghnani, M. & Secco, R. A Modified Ultrasonic Interferometer for Sound-Velocity Measurements in Molten Metals and Alloys. *Rev. Sci. Instrum.* **65,** 682–688 (1994).
[57] Thevenard, D. & Benhadid, H. Low Prandtl Number Convection in a Rectangular Cavity with Longitudinal Thermal-Gradient and Transverse G-Jitters. *Int. J. Heat Mass Transf.* **34,** 2167–2173 (1991).
[58] Rivière, N., Travin, G. & Perkins, R. J. Subcritical open channel flows in four branch intersections. *Water Resources Research* **47,** W10517 (2011).
[59] Eckert, S., Gerbeth, G. & Melnikov, V. I. Velocity measurements at high temperatures by ultrasound Doppler velocimetry using an acoustic wave guide. *Experiments in Fluids* **35,** 381–388 (2003).
[60] Inatomi, Y., Onishi, F., Nagashio, K. & Kuribayashi, K. Density and thermal conductivity measurements for silicon melt by electromagnetic levitation under a static magnetic field. *International Journal of Thermophysics* **28,** 44–59 (2007).
[61] Hayashi, M., Yamada, H., Nabeshima, N. & Nagata, K. Temperature dependence of the velocity of sound in liquid metals of group XIV. *International Journal of Thermophysics* **28,** 83–96 (2007).

[62] Rhim, W. K. & Ohsaka, K. Thermophysical properties measurement of molten silicon by high-temperature electrostatic levitator: density, volume expansion, specific heat capacity, emissivity, surface tension and viscosity. *Journal of Crystal Growth* **208,** 313–321 (2000).
[63] Garandet, J. P. New Determinations of Diffusion Coefficients for Various Dopants in Liquid Silicon. *International Journal of Thermophysics* **28,** 1285–1303 (2007).
[64] Sobolev, V. Institutional Repository of the Belgian Nuclear Research Centre (SCK-CEN): Database of thermophysical properties of liquid metal coolants for GEN-IV. *http://publications.sckcen.be/dspace/handle/10038/7739* (2011).
[65] Okhotin, A. S., Pushkarskii, A. S. & Gorbachev, V. V. Thermophysical Properties of Semiconductors. *Atomizdat, Moscow* (1972).